Andraž Kontarček, Mitja Nemec, Primož Bajec, Vanja Ambrožič

Single Open-phase Fault Detection with Fault-Tolerant Control of an Inverter-fed Permanent Magnet Synchronous Machine

Original scientific paper

In this paper first a current predictive method for single open-phase fault detection in a three phase drive with a permanent magnet synchronous machine is presented. The proposed method is based on a predictive stator current calculation. For each sampling interval the difference between the actual stator current and its predicted value in a previous sampling interval is calculated. To identify the location of a single open-phase fault, an identification method is presented which is based on the analysis of the stator current vector angle. After the single open-phase fault is detected and identified it is desirable for the electrical machine to continue operating with a reduced number of phases. For this purpose, a modified direct torque control algorithm for the fault-tolerant control is implemented. In order to improve the performance of the drive, a pre-firing angle is additionally introduced. All proposed methods have been simulated in Matlab/Simulink and verified on an experimental model.

Key words: Permanent magnet synchronous machine, Fault-tolerant-system, Single open-phase fault, Fault-tolerant control, Pre-firing angle

Detekcija odspojene faze i na kvarove otporno upravljanje pretvaračem napajanim sinkronim motorom s permanentnim magnetima. U članku je prvo predstavljena metoda za detekciju kvara odspojene faze u tro-faznom elektromotornom pogonu sa sinkronim motorom s permanentim magnetima zasnovana na predikciji struja statora. U svakom koraku uzorkovanja računa se razlika između trenutne mjerene struje statora i prediktirane vrijednosti iz prethodnog koraka. U svrhu određivanja lokacije odspojene faze, predstavljena je metoda identifikacije zasnovana na analizi kuta vektora struje statora. Nakon otkrivene i utvrđene odspojene faze, poželjno je nastaviti rad električnog stroja sa smanjenim brojem faza. U ovu svrhu implementiran je izmijenjeni algoritam izravnog upravljanja momentom za postizanje na kvarove otpornog upravljanja. Da bi se unaprijedilo vladanje sustava elektromotornog pogona, dodatno je uveden kut prethođenja aktivacije impulsa. Sve predložene metode simulirane su u Matlab/Simulink okruženju i provjerene na eksperimentalnom postavu.

Ključne riječi: Sinkroni motor s permanentnim magnetima, na kvarove otporan sustav, kvar jedne odspojene faze, na kvarove otporno upravljanje, kut prethođenja aktivacije impulsa

1 INTRODUCTION

Permanent magnet synchronous machines (PMSM) are widely used in different kind of applications due to their efficiency and high torque per mass ratio [1,2]. Along with the development of modern power electronics and microprocessor technology, more advanced control methods for electrical drives have been developed. Nowadays, two standard control strategies for PMSMs are mainly used, namely field-oriented control (FOC) and direct torque control (DTC) [3-8], which compete with predictive approaches [9-11].

With the growing complexity of machine drives, the probability of system failures increases. For such a system it is desirable to detect different kinds of faults and, if possible, to continue operating after the fault occurs. Fault detection and fault-tolerant control are two functionalities of the modern controlled system, also known as the "fault-tolerant system".

There are many different types of faults that may occur in electrical drives. A report on the faults of variable speed AC drives [12] shows that 38% of faults are located in power switching devices, 53.1% in control circuits and 7.7% in external auxiliaries. Different sensor faults such as encoder fault, DC-link voltage, and current sensor faults are discussed in [13]. Most common power converter faults are: a single transistor short circuit, a phase-leg short circuit, open-phase, a loss of driving signal, a capacitor short circuit fault, and a two or three phase short circuit [14-

16]. Although there are many different types of faults that may occur in a power converter driven system, in this paper only the single open-phase fault (SOPF) will be discussed (Fig. 1). With this type of fault one of the machine's phases is completely disconnected, either at the machine terminals or within the power converter.
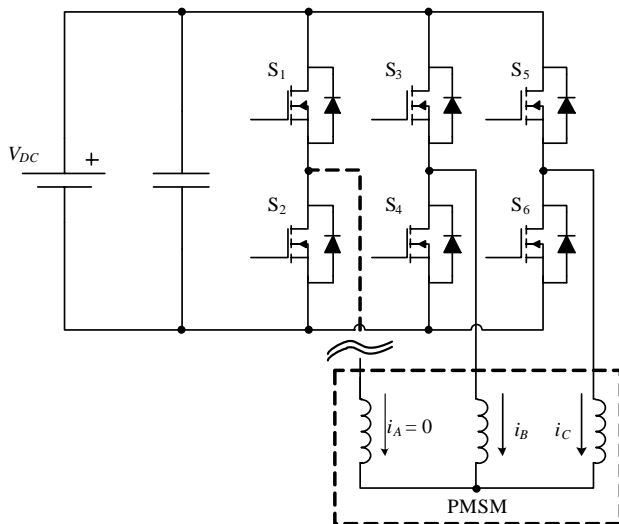

Fig. 1. Power converter topology in case of SOPF

A survey of various fault detection methods is presented in [17] where 21 methods for open-circuit faults and ten methods for short-circuit fault detection are discussed.

Transistor gate-misfiring faults are briefly discussed. In [18], a technique for detecting an open-circuit fault (based on Park's vector approach) is considered. Other methods for detecting transistor open-circuits and short-circuits have been presented in [19-22].

In [23], two solutions for open-phase detection are presented. The first one is based on a harmonic analysis of PMSM stator currents. More specifically, in the case of a SOPF the frequency spectrum of stator currents changes, which can be detected by the proposed method. The second method is based on a machine current signature analysis (MCSA) by comparing the trajectories of the current space vector. The main disadvantage of these two methods is their slowness, since they require monitoring of the stator current for at least one electrical period (after the occurrence of the fault) for proper and unambiguous fault detection.

The fault-tolerant control is also very important from the point of view of safety. In many applications the most critical variable to be controlled is the electromagnetic torque (also when having a superimposed speed control loop). In [24-26] a modified DTC method for fault-tolerant control of a four-switch inverter is proposed. Similar hardware topology was presented in [27] but, instead of DTC,

a FOC strategy with space vector modulation (SVM) was used. Hardware solutions with additional phase or neutral leg topologies are presented in [16, 28-30]. Paper [31] compares both DTC and FOC methods with additional leg and neutral leg topologies. In [32], the complete functionality of "fault-tolerant system" is presented, including fault detection, isolation and fault-tolerant control of PMSM. The main disadvantage of all these solutions is that the electric circuitry needs to be changed after the occurrence of the fault, which increases the complexity of the power converter, as well as its size and costs. Furthermore, in some solutions the neutral point of the machine has to be accessible.

In the most critical applications, "fault-tolerant systems" are multiphase ones [33, 34] which require special machine construction as well as power converter architectures. However, due to the additional weight and costs the multiphase systems are not the appropriate solution in some applications [35].

In the presented paper the main goal is implementation of the "fault-tolerance" concept for an ordinary three-phase synchronous machine drive without adding any additional hardware.

Here, the DTC method is used as a controlling method, while a SOPF is detected using the predictive current method. Predictive current detection method theory applies in general for different types of faults, but in this paper only detection of a SOPF is discussed. The proposed method is based on a predictive stator current calculation and the analysis of an error vector. After a SOPF is detected the SOPF identification is also necessary. Therefore, an identification method based on an analysis of the stator current vector angle is presented. With the proposed method the SOPF location can be unambiguously identified.

The second important part of "fault-tolerant system" is the fault-tolerant control with a reduced number of phases, which is also presented in this paper. The main advantages of the proposed method are that the topology of the complete circuit remains the same as before the failure and that there is also no need to have the machine's neutral point accessible. However, the proposed method is intended for the continuing operation of an already running machine until a safe stop.

2 MATHEMATICAL MODEL OF PMSM

The electrical equations that describe a general PMSM model in a rotor flux *d-q* reference frame can be expressed as [2]:

$$\lambda_{Sd} = L_{Sd}i_{Sd} + \lambda_{PM}, \qquad (1)$$

$$\lambda_{Sq} = L_{Sq}i_{Sq}, \qquad (2)$$

$$v_{Sd} = L_{Sd}\frac{di_{Sd}}{dt} + R_S i_{Sd} - \omega_{el}L_{Sq}i_{Sq}, \qquad (3)$$

$$v_{Sq} = L_{Sq}\frac{di_{Sq}}{dt} + R_S i_{Sq} + \omega_{el}L_{Sd}i_{Sd} + \omega_{el}\lambda_{PM}, \quad (4)$$

where v_{Sd} and v_{Sq} are stator voltages, λ_{Sd} and λ_{Sq} stator flux linkages, i_{Sd} and i_{Sq} stator currents and L_{Sd} and L_{Sq} stator inductances. R_S is the stator phase resistance, λ_{PM} the permanent magnet flux linkage and ω_{el} is the electrical angular speed of the rotor. The electrical angular speed of the rotor (ω_{el}) and electrical rotor angle (θ_{el}) are aligned with the rotor flux speed and rotor flux angle - ω_{el} and θ_{el} will be used in the following sections.

Electromagnetic torque can be written as:

$$\tau_{el} = \tfrac{3}{2}p \cdot \big(\lambda_{PM}i_{Sq} + (L_{Sd} - L_{Sq})i_{Sd}i_{Sq}\big), \quad (5)$$

where p is the number of pole pairs.

3 DTC CONTROL METHOD

Direct torque control is an alternative to field-oriented control. Here, mathematical transformations to the field coordinate system are not necessary so the complexity of the calculation is lower. Both flux and torque are directly controlled by using hysteresis controllers in stator coordinates. The conventional DTC [36] method takes into account the final inverter states so the output voltages are not modulated directly. The output voltage vectors are selected from a look-up table. Compared to a FOC only one voltage vector is applied to the machine during the sampling interval. A block diagram of the conventional DTC is shown in Fig. 2.
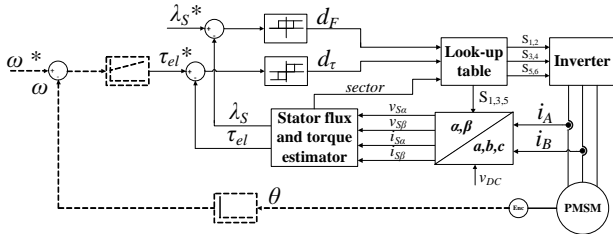

Fig. 2. Conventional DTC scheme for PMSM

Here, v_{DC} is the DC-link voltage, * denote the reference values for speed, electromagnetic torque and flux. Stator voltages $v_{S\alpha}$ and $v_{S\beta}$ in the $\alpha\beta$ - reference frame are reconstructed from the DC-link voltage v_{DC} and transistor switching states. The look-up table for the conventional DTC is given in Table 1 [35]. The flux controller is a two-level hysteresis controller, where $d_F = 1$ means "increase flux" and $d_F = -1$ means "decrease flux". For controlling torque, a three-level hysteresis controller is used, where $d_\tau = 1$ means "increase torque", $d_\tau = -1$ means "decrease torque" and $d_\tau = 0$ means "no torque change". Sectors 1 to 6 are determined by the stator flux vector position.

Table 1. Conventional DTC look-up table

Controller output \ Sector		1	2	3	4	5	6
$d_F = 1$	$d_\tau = 1$	V_2	V_3	V_4	V_5	V_6	V_1
	$d_\tau = 0$	V_7	V_0	V_7	V_0	V_7	V_0
	$d_\tau = -1$	V_6	V_1	V_2	V_3	V_4	V_5
$d_F = -1$	$d_\tau = 1$	V_3	V_4	V_5	V_6	V_1	V_2
	$d_\tau = 0$	V_0	V_7	V_0	V_7	V_0	V_7
	$d_\tau = -1$	V_5	V_6	V_1	V_2	V_3	V_4

4 PREDICTIVE SOPF DETECTION METHOD

The proposed method for SOPF detection is based on a predictive calculation of the stator current in the next sampling interval [37]. If the sampling interval is small enough (in our case 50 μs), some simplifications can be introduced; ω_{el} can be considered to be quasi-constant and the stator currents change almost linearly (not exponentially) during the whole sampling interval. Therefore, voltage equations (3) and (4) can be discretized using the Euler approximation method, thus enabling the prediction of the stator current [8,10]:

$$\begin{aligned}\hat{i}_{Sd}(n + 1) = {}& i_{Sd}(n)\left(1 - \tfrac{R_S}{L_{Sd}}\Delta t\right) + \\ & + \omega_{el}(n)\tfrac{L_{Sq}}{L_{Sd}}\Delta t \cdot i_{Sq}(n) + \tfrac{\Delta t}{L_{Sd}}v_{Sd}\end{aligned}, \quad (6)$$

$$\begin{aligned}\hat{i}_{Sq}(n + 1) = {}& i_{Sq}(n)\left(1 - \tfrac{R_S}{L_{Sq}}\Delta t\right) - \\ & - \omega_{el}(n)\tfrac{L_{Sd}}{L_{Sq}}\Delta t \cdot i_{Sd}(n) - \\ & - \omega_{el}(n)\tfrac{\lambda_{PM}\Delta t}{L_{Sq}} + \tfrac{\Delta t}{L_{Sq}}v_{Sq}\end{aligned}, \quad (7)$$

where index n denotes a consecutive number of sampling interval and Δt is a duration of the sampling interval.

Since R_S, λ_{PM}, L_{Sd} and L_{Sq} are machine parameters it can be assumed that they do not change during operation. In reality, both resistances and inductances are not constant, but this change does not significantly influence the predictive method used in this paper as shown in [38]. Angular speed ω_{el} and stator currents i_{Sd} and i_{Sq} are measurable values, while voltages v_{Sd} and v_{Sq} can be determined by the switching states of transistors and the DC-link voltage.

With no failure in the machine drive system, it can be assumed that actual values of currents in $(n + 1)$-th sampling interval will just slightly deviate from the calculated ones out of equations (6) and (7). On the other hand, if any failure in the system occurs, the deviation between the measured and calculated current in $(n + 1)$-th sampling interval should become larger. Consequently, an error (ε) can be calculated as a difference between the actual current in the $(n + 1)$-th sampling interval and the predicted current

in $(n + 1)$-th sampling interval, which was calculated in previous sampling interval:

$$\varepsilon_d(n + 1) = i_{Sd}(n + 1) - \hat{i}_{Sd}(n + 1), \qquad (8)$$

$$\varepsilon_q(n + 1) = i_{Sq}(n + 1) - \hat{i}_{Sq}(n + 1). \qquad (9)$$

In order to encompass errors in both coordinates, a magnitude of error vector will be used for further analysis:

$$\varepsilon(n + 1) = \sqrt{\varepsilon_d^2(n + 1) + \varepsilon_q^2(n + 1)}. \qquad (10)$$

Stator current and error vectors are shown in Fig. 3. Vector $i_S(n)$ presents the stator current in the sampling interval before the SOPF occurs; $\hat{i}_S(n + 1)$ is the predicted current for the next sampling interval as if there is no failure in the system and is calculated in the previous interval (before the SOPF). The actual currents for both unaffected phases at the instant of SOPF are $i_{Sa}(n)$ and $i_{Sb}(n)$, the faulty phase current $i_{Sc}(n)$ is not depicted since it is equal to zero. The vector $i_S(n + 1)$ denotes the actual stator current at the instant of SOPF (vector sum of unaffected phases). The stator current angle δ is depicted as well, since it will be used later for SOPF identification. Additionally, an error vector $\varepsilon(n + 1)$ is shown as a difference between the vectors $i_S(n)$ and $\hat{i}_S(n)$.

Fig. 3. Current and error vectors in rotor coordinates at the instant of SOPF

If the machine operates under normal conditions and there is no fault in the system, the absolute error magnitude $\varepsilon(n + 1)$ is relatively small and always within its normal condition range. If any failure in the power converter occurs, the error magnitude will exceed the error threshold (11). The error threshold (ε_{fault}) is hard to define analytically as it depends on numerous factors (inaccuracy in currents measurements, machine and inverter parameters, sampling time, etc.) and was therefore determined experimentally. The error threshold can be chosen as three times

of the maximum error magnitude $\varepsilon(n + 1)$ at machine's operation without fault.

The increase of the error magnitude can be quickly detected in a few sampling intervals.

$$\varepsilon(n + 1) > \varepsilon_{fault}. \qquad (11)$$

Accurate estimation of voltages is essential for an accurate, predictive current calculation in (6) and (7). Instead of measuring them the voltages are determined by the switching states of transistors and the DC-link voltage. These phase voltages differ from the actual voltages due to influences such as parasitic inductances, dead-time effects, nonlinearities, voltage drops on switching devices, etc. However, phase voltages could be more accurately estimated by measuring the temperatures on the elements in the circuitry [39]. Therefore, the voltage drops on the elements may also be taken into account for the estimation. Since the conventional DTC has a maximum of one switching state during one switching interval these parasitic effects are usually minimal.

5 SOPF IDENTIFICATION

After a SOPF is detected, the identification of the fault is also necessary. By analyzing the angle of the stator current vector at the instant of fault the SOPF location can be unambiguously identified. There are two possible situations for each phase that may occur at the instant of a SOPF. In both situations the faulty phase current falls to zero while the other two phase currents have the same value of the current, but with the opposite polarity (one phase current has positive sign, the other has negative and vice versa). So, in case of a SOPF, there are in total six combinations of stator current vectors possible - two for each phase.

When analyzing the current vectors at the instant of a SOPF (Fig. 3), it can be clearly seen that the faulty phase current vector is zero, while the two remaining current vectors have the same magnitude. The vector sum of other two phase current vectors is vector $i_S(n + 1)$ with angle δ. The value of angle δ is always the same in one situation regardless of the magnitudes of the remaining two phase currents. Therefore, by calculating the angle of the stator current at the instant of the fault, the SOPF location can be unambiguously determined. In Table 2 all possible combinations of a SOPF for particular angles are presented. The values in Table 2 are theoretical angles for each faulty phase. However, in practice, due to the effects caused by discretization, instead of using the exact values, some intervals need to be defined due to measurement uncertainty. Note that these intervals can be very large (e.g. 10 degrees), as the theoretical angles are far apart.

Table 2. SOPF identification.

Stator current angle δ [°]	Faulty phase
90 or 270	phase A
30 or 210	phase B
150 or 330	phase C

6 FAULT-TOLERANT CONTROL WITH A RE-DUCED NUMBER OF PHASES

After a SOPF is detected and identified, the continuation of operation with reduced torque is desirable. Usually, the inverter and machine topologies, designed especially for such kind of operation, provide a type of redundancy [16,28]. In this study the conventional inverter topology using only three transistor phase legs has been investigated, thus trying to offer the fault detection and fault-tolerant control capabilities to regular and most common drives.

6.1 The modified DTC

A major advantage of the proposed solution is that the topology of the power converter circuit does not change after the fault occurs. Another significant advantage is that there is no need for the machine's neutral point to be accessible. Therefore, only the control algorithm has to be modified, making this solution very cost effective, too [40].

When a SOPF occurs the transistor leg to which the faulty phase winding was connected becomes inactive. Consequently, there are only two active and two zero voltage vectors available, compared to six active voltage vectors in a fully-functional power converter. Those two active vectors are always perpendicular to the faulty phase. In the conventional DTC there are six sectors which are determined by the stator flux angle. The modified DTC has only two sectors available and they can be determined by electrical rotor angle, thus basically forcing the machine into single-phase operation.

As already mentioned the proposed solution is cost effective with the drawback of reduced functionality since it is not guaranteed that the machine can start once it has stopped due to the presence of the fault.

Fig. 4 shows possible voltage vectors in the case when phase A is opened. Active vector $\mathbf{V}_{BC}$ is depicted at 90 rotor electrical degrees and the other active vector $\mathbf{V}_{CB}$ at 270 rotor electrical degrees. The area on the right side can be labeled with sector I and the area on the left side with sector II. For example, if the rotor flux is located in sector I and voltage vector $\mathbf{V}_{BC}$ is impressed, the electromagnetic torque will increase. On the other hand, if the rotor flux is located in sector I and vector $\mathbf{V}_{CB}$ is impressed, the electromagnetic torque will decrease. The situation is opposite if the rotor flux is located in sector II. By impressing the zero vector $\mathbf{V}_0$ in both sectors, the electromagnetic

torque will not change. If the rotor flux is located very close to the boundaries of the sectors (around 90 or 270 electrical degrees) the machine generates a very small torque. Therefore, if the machine stops with the rotor flux near the boundary it will be almost impossible to start it again, since the maximum current is limited.

The voltage equations can be simplified as follows (after neglecting resistance voltage drop):

$$V_S = 2 \cdot L_S \frac{di_S}{dt}, \qquad (12)$$

where V_S denotes the amplitude of the active voltage vector (in our case V_{BC} or V_{CB}) and i_S the stator current ($i_S = i_B = -i_C$).

With the proposed method the electromagnetic torque is controlled by a hysteresis torque controller with two active and one zero vector. Since the number of degrees of freedom is reduced, the stator flux is no longer directly controlled. The maximum achievable torque and power depend on the hardware setup (maximum inverter current, maximum machine current, effective machine current etc.) and constraints dictated by the application.

Beside the representation in vector diagrams, Fig. 4 also contains a look-up table for opened phase A, where θ_{el} is the electrical angle, d_τ is the hysteresis torque controller output, where $d_\tau = 1$ means "increase torque", $d_\tau = -1$ means "reduce torque" and $d_\tau = 0$ "no torque change".

The modified DTC scheme is shown in Fig. 5.

Electrical angle / d_T	$270° \le \theta_{el} < 90°$ (Sector I)	$90° \le \theta_{el} < 270°$ (Sector II)
$d_\tau = 1$	V_{BC}	V_{CB}
$d_\tau = 0$	V_0	V_0
$d_\tau = -1$	V_{CB}	V_{BC}
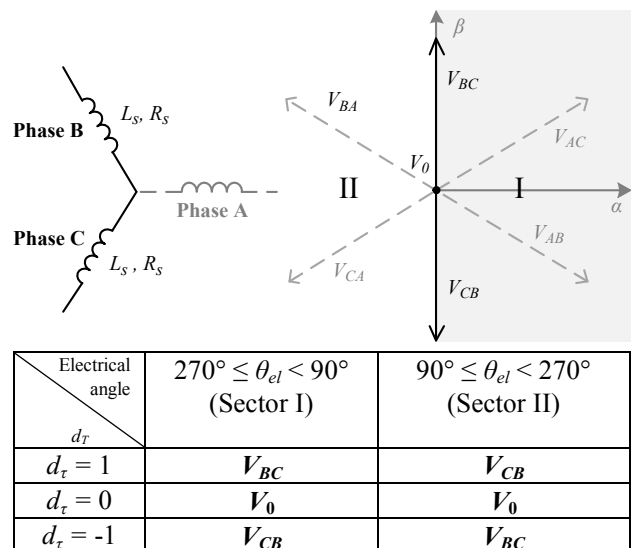
Fig. 4. Voltage vectors and a modified look-up table for opened phase A

6.2 The pre-firing angle

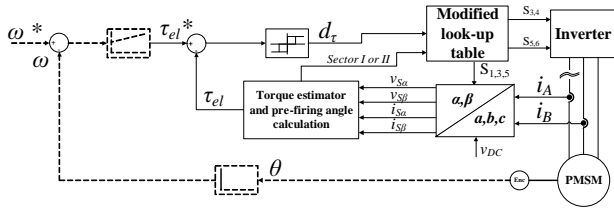As it is shown in this chapter, the electrical machine operating with a reduced phase can produce negative torque

Fig. 5. Fault-tolerant modified DTC scheme in case of opened phase A

Fig. 6. Stator currents (top) and electromagnetic torque (bottom) at different pre-firing angles

when the rotor flux is changing sectors, which is not desirable in motor operation mode. This negative torque causes undesirable temporary braking, which increases the stress on key mechanical parts of the electrical machine. For this purpose a time instant when the switching between two active voltage vectors occurs is evaluated and described in detail. The case considers a SOPF for phase A. Similar considerations also apply for the other two phases.

Theoretically, the instant for switching of voltage vectors occurs at two particular electrical rotor angles: at 90 and 270 electrical degrees (Fig. 4). Since stator inductances are not negligible, the stator current does not change its polarity immediately, but gradually decreases to zero instead. Consequently, the stator current changes its polarity a few electrical degrees later than would be desirable. During the time between the instant in which the rotor flux changes sectors and the moment when the current falls to zero, the stator current is still positive but the electromagnetic torque becomes negative. Therefore, the positive current causes negative torque, which is not desirable. This phenomena also decreases the mean value of torque, thus deteriorating the overall performance. In order to solve this issue, a control algorithm should commutate voltages prior to the theoretical moment of switching (pre-firing).

In Fig. 6 the stator current and torque are depicted in the time instant of switching of voltage vectors. Both the stator current and torque are presented for different pre-firing angles. It can be noticed that without pre-firing, the stator current actually changes its direction at 280 electrical degrees which is 10 degrees after the theoretical switching angle (270 electrical degrees). If the proper pre-firing angle is introduced (θ_{pf}) the current changes its sign very closely to the theoretical angle θ_{sw}. Consequently, the electromagnetic torque will always be positive. In the case of premature pre-firing, the electromagnetic torque becomes negative as well, so it is important for the pre-firing angle to be determined accurately.

For an easier explanation of the pre-firing angle calculation, two time instants are introduced as shown in Fig. 6: point A indicates the moment of switching between voltage vectors (at angle θ_{pf}) and point B indicates the moment at switching angle (at angle θ_{sw}) when the stator cur-

rent should fall to zero. Also, two time variables are introduced: time t_{el} in which the current would fall to zero and time t_{meh} in which rotor gets into the position of optimal switching angle (in this case 90 and 270 rotor electrical degrees). If the rotor resistances are neglected (since the stator current decreases almost linearly to zero), the exact time t_{el} in which the current would fall to zero can be calculated using the following equation:
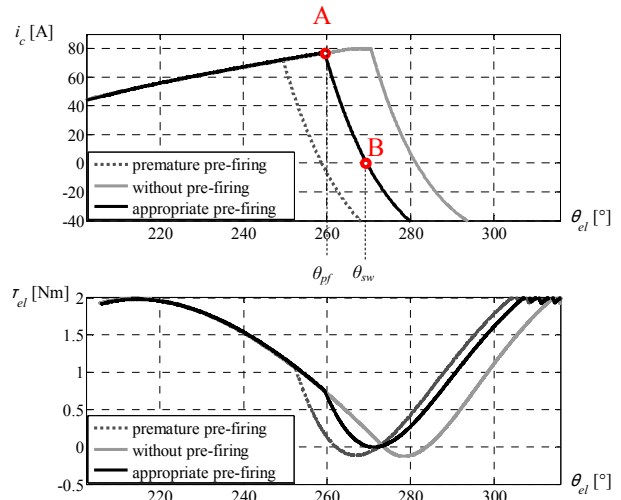
$$dt = \frac{2 \cdot L_S}{V_{DC} - e_{EMF(B-C)}(t)} di_C, \qquad (13)$$

where i_C denotes the measured stator current, V_{DC} the DC-link voltage, $e_{EMF(B-C)}$ denotes phase to phase back EMF voltage, and L_S denotes the stator inductance. Back EMF voltage between phases B and C can be expressed as:

$$e_{EMF(B-C)}(t) = K \cdot \cos(\omega_{el}t). \qquad (14)$$

In the immediate proximity of switching vectors (at 90 and 270 degrees), the back EMF voltage is small compared to V_{DC}, so it does not significantly influence the current slope. Therefore, if the back EMF voltage is neglected, the equation (13) can be further simplified and discretized as follows:

$$t_{el} \cong \frac{2 \cdot L_S \cdot i_C}{V_{DC}}. \qquad (15)$$

Taking into account the measured electrical rotor angle θ_{el}, the theoretical switching angle $\theta_{sw}(90° \text{ and } 270°)$, and the electrical angular speed ω_{el}, the time in which the rotor will get in the position of the switching angle θ_{sw} can be calculated as:

$$t_{meh} = \frac{\theta_{sw} - \theta_{el}}{\omega_{el}}. \qquad (16)$$

When the values of t_{el} and t_{meh} are equal, the voltage vectors should be switched. Assuming that the time variables are accurately calculated, the following criteria (due to discretization) can be introduced:

$$t_{meh} - t_{el} < \frac{\Delta t}{2}. \qquad (17)$$

If (17) is not fulfilled, there is still enough time remaining to switch the voltage vectors. Therefore, voltage vectors should not be switched in the instantaneous sampling interval, and the above procedure has to be repeated in the next sampling interval. In the case that equation (17) is fulfilled the voltage vectors should be switched.

7   SIMULATION RESULTS

At first, the fault detection, identification and fault-tolerant control were simulated in a MATLAB/Simulink simulation environment, where the SimPowerSystem package was used for simulation of the power converter and the machine.

All of the following simulations were performed at a constant reference speed of 600 rpm and a reference load torque of 0.5 Nm. The parameters of the simulated and tested machine are given in Table 3.

<div align="center">

Table 3. Machine parameters.

$R_S = 56.7 \text{ m}\Omega$	$p = 3$
$L_{Sd} = 68 \ \mu\text{H}$	$\lambda_{PM} = 9.3 \text{ mWb}$
$L_{Sq} = 86 \ \mu\text{H}$	$f_s = 20 \text{ kHz}, \Delta t = 50 \ \mu\text{s}$
$P = 0.2 \text{ kW}$	$I_S = 30 \text{ A}$

</div>

In Fig. 7, phase A (drawn in black) is opened at 0.02 s with a rotor electrical angle of 90 degrees and phase current at its peak. After a SOPF occurs, the faulty phase current falls to zero, while the other two phase currents become phase shifted by 180 degrees. Fig. 8 presents the magnitude of the error vector ε. It is obvious that its value significantly increases after a SOPF occurs.

Figs. 9 and 10 show stator currents, the electrical rotor angle, and the error magnitude when phase A is opened at the minimum value of the phase current at 0 degrees of the electrical rotor angle.

It can be seen that the error magnitude ε depends on the value of the stator current through the phase winding before the fault occurs. If the phase opens at the moment when the phase current is at its peak, the error magnitude ε will also be high. On the contrary, if the phase opens while the current through the faulty phase is close to zero the error magnitude will be small and the increase of the error magnitude will be harder to detect. Those two operating points are chosen intentionally to prove the validity of the method at two boundary conditions.
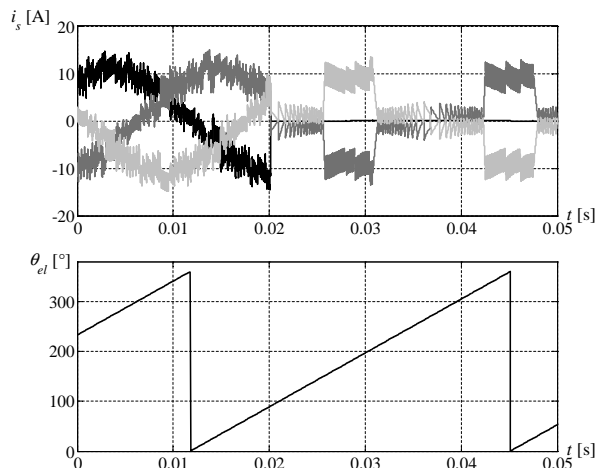
Fig. 7. Simulations of stator currents and the electrical rotor angle; phase A is opened at the maximum value of the phase current
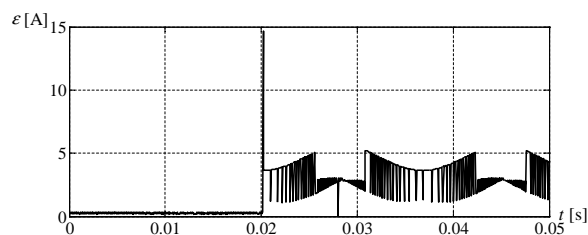
Fig. 8. Simulation of error magnitude ε; phase A is opened at the maximum value of the phase current
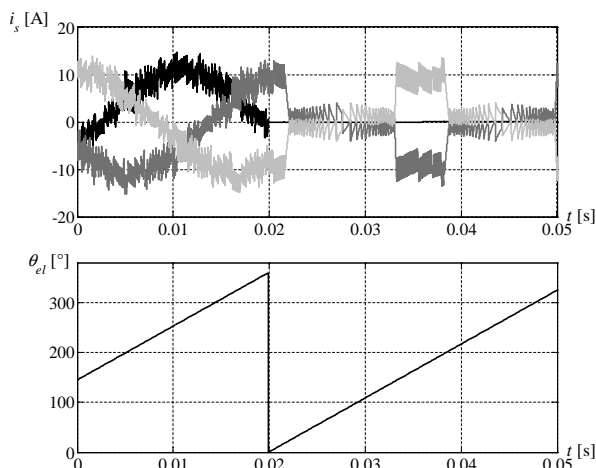
Fig. 9. Simulations of stator currents and electrical rotor angle; phase A is opened at the minimum value of the phase current

After fault detection and identification, the fault-tolerant control mode has also been simulated. Fig. 11
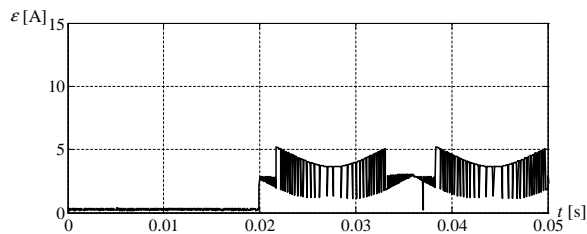
Fig. 10. Simulation of error magnitude ε; phase A is opened at the minimum value of the phase current
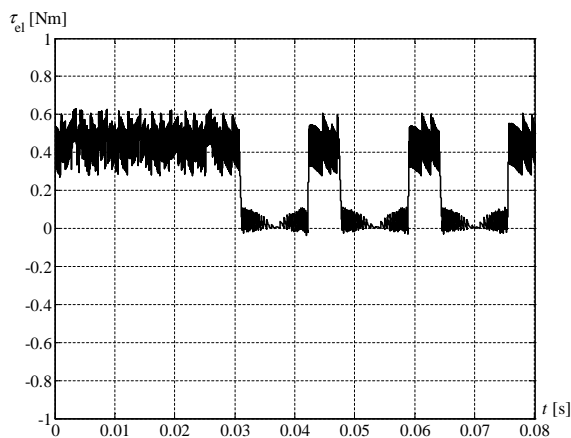

Fig. 11. Simulation of electromagnetic torque (SOPF occurs at 0.03 s) without modifying the DTC algorithm
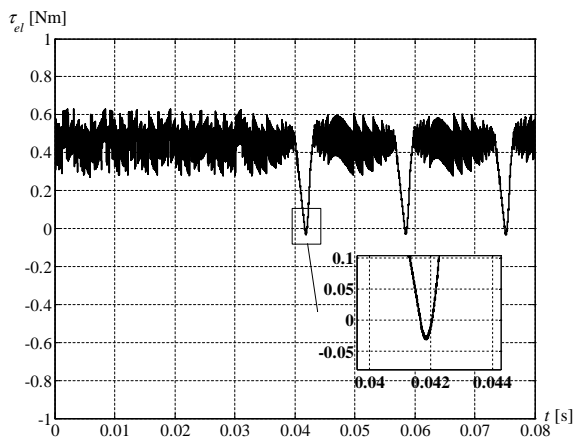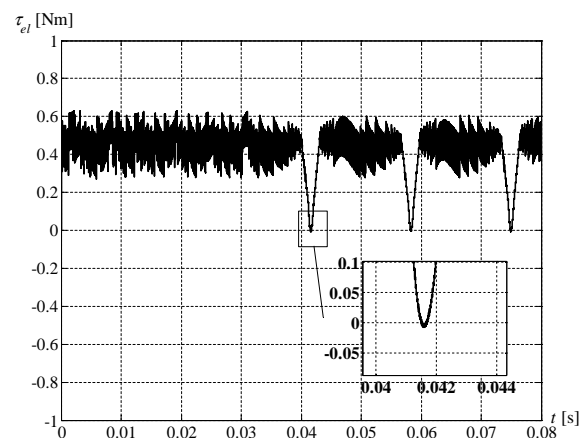

Fig. 12. Simulation of electromagnetic torque (SOPF occurs at 0.03 s) with a modified DTC algorithm and no pre-firing angle included

presents the electromagnetic torque without modifying the DTC table (DTC algorithm operates as if no SOPF has been detected). The reference value of torque was set

Fig. 13. Simulation of electromagnetic torque (SOPF occurs at 0.03 s) with a modified DTC algorithm and with a pre-firing angle

to 0.5 Nm; the rotational speed was constant and set to 600 rpm. In this case the machine achieves the reference value of the torque only temporarily. The mean value of the torque significantly decreases (by 71 percent) to 0.13 Nm.

When a SOPF is detected and identified the control algorithm is modified, as described previously. Even if the pre-firing angle is not introduced the mean torque increases significantly to 0.41 Nm. But, problems still persist around zero torque where the torque becomes negative, as shown in Fig. 12.

Optimal results are achieved with a combination of the modified DTC look-up table and the accurate pre-firing angle (Fig. 13). Consequently, the mean torque reaches 0.42 Nm.

The negative torque produced by the machine during switching of the voltage vectors is particularly noticeable at higher speeds (Fig. 14). Here, the importance of the introduction of the pre-firing angle is significant. In Fig. 15 the post-fault torque with a modified DTC and included pre-firing angle is presented, with the reference speed set to 1200 rpm and with a 0.5 Nm of load torque. It can be seen that the pre-firing angle is also accurately calculated at higher speeds. This confirms the assumption that the EMF voltage does not have significant impact on the estimation of time required for the phase current to fall to zero.

In Fig. 16 a torque-speed graph is presented. Two simulations were made, without a fault and after a SOPF, at the constant stator current of 30 A RMS. It can be seen that drive is derated to 50%.

8 EXPERIMENTAL RESULTS

To confirm the "fault-tolerant" theory and simulation results the proposed methods were additionally verified on

481
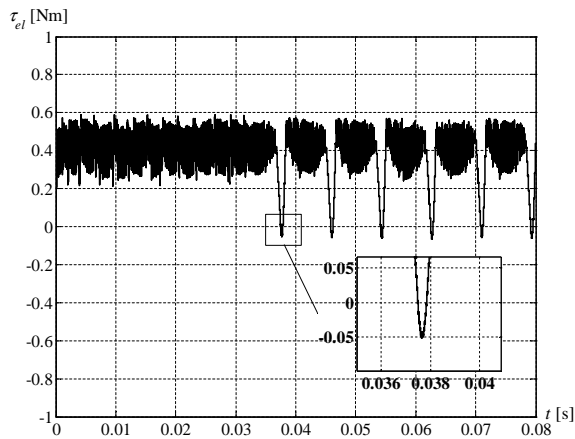
Fig. 14. Simulation of electromagnetic torque at speed reference 1200 rpm, with a modified DTC table and without using a pre-firing angle
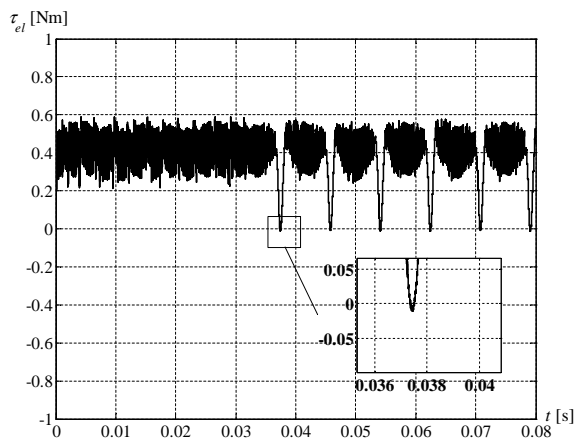

Fig. 15. Simulation of electromagnetic torque at speed reference 1200 rpm, with a modified DTC table and the pre-firing angle included
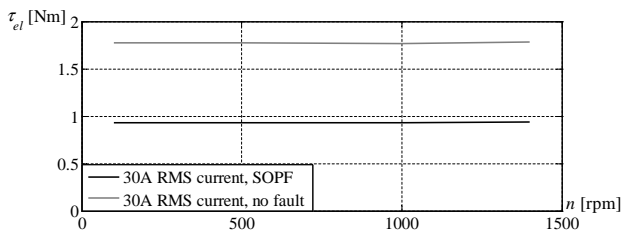

Fig. 16. Torque-speed graph at 30 A RMS stator current

an experimental setup. The setup consists of two PMSM machines on a common shaft. The first machine is controlled with its own and independent power converter,

maintaining the constant rotational speed either in the motor or generator mode. The other machine is used for the testing of the proposed innovative method. For the implementation of all proposed algorithms a TMS320F28069 microcontroller was used. Generation of open-phase faults is done by means of a custom-designed phase breaker, namely a microprocessor triggered switch, so the phase can be opened in any rotor angle.

In Figs. 17 and 18 stator currents, the electrical rotor position and error magnitude ε are shown when phase A opens at the maximum value of the phase current (at rotor electrical position of 90 degrees). The error is clearly visible, and consequently the implemented and previously described algorithm for SOPF detection and identification easily identifies which phase is opened.

In order to test the sensitivity of the identification algorithm another measurement was preformed, this time with phase A being opened at the minimum value of the phase current (at rotor electrical angle of 0 degrees). The measurement results are shown in Figs. 19 and 20.

In this case the error magnitude ε is smaller than in the previous case, but still high enough to detect the fault, especially if it is monitored for a few consecutive intervals. After the occurrence of the SOPF, the value of error magnitude ε can occasionally drop below the normal condition range, but once the SOPF is detected, the error magnitude is not monitored anymore. Note that the case shown in the figure is only for demonstration purposes, as it shows the ongoing curves if the fault was not detected and the appropriate control action undertaken.

It can also be seen that experimental results match the simulation ones very well. Nevertheless, if the error signal
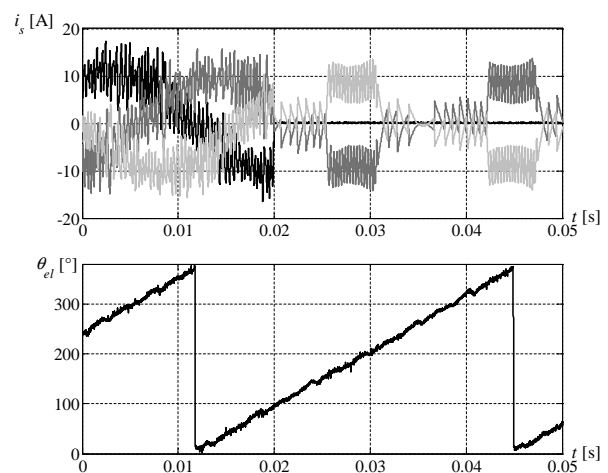

Fig. 17. Measurement results of stator currents and the electrical rotor angle; phase A is opened at the maximum value of the phase current
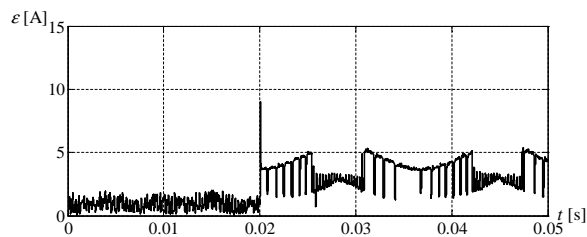
Fig. 18. *Measurement results of error magnitude ε; phase A is opened at the maximum value of the phase current*
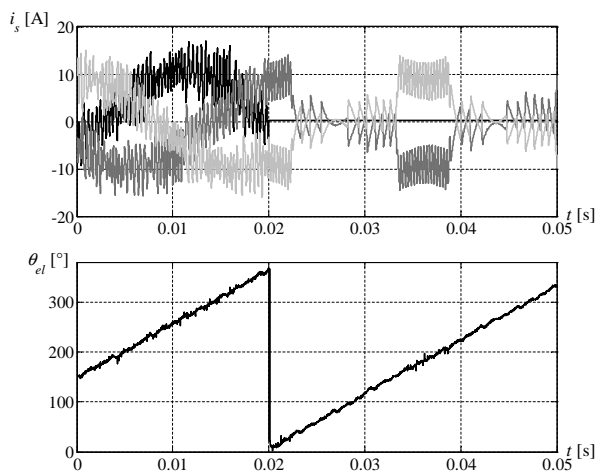

Fig. 19. *Measurements results of stator currents and electrical rotor angle; phase A is opened at the minimum value of the phase current*
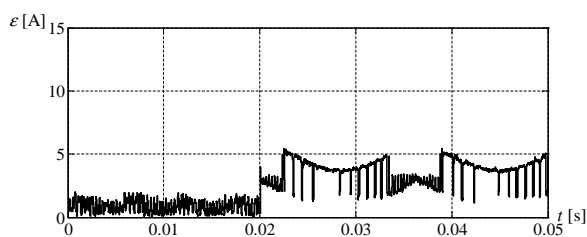

Fig. 20. *Measurement results of error magnitude ε; phase A is opened at the minimum value of the phase current*

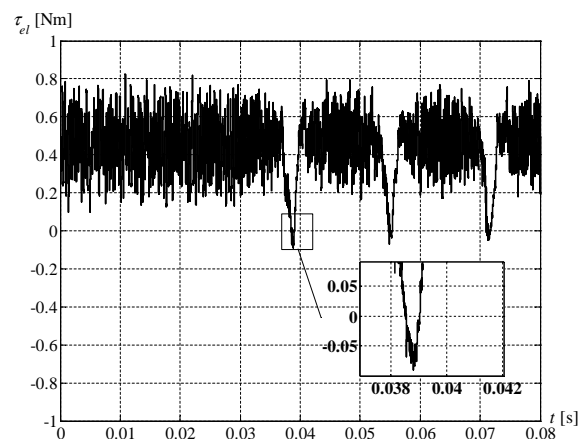Fig. 21. *Measurement results of electromagnetic torque (SOPF occurs at 0.03 s) without modifying the DTC algorithm*

Fig. 22. *Measurement results of electromagnetic torque (SOPF occurs at 0.03 s) with a modified DTC algorithm and no pre-firing angle included*

before a SOPF occurrence is observed (Figs 18 and 20), additional noise is noticed not present in the simulations (Figs. 8 and 10). This difference is owed to the noise in the measurements of the stator currents and the inaccurate estimation of impressed stator voltages, which are present in any real system.

After the experimental system detects and identifies a SOPF, it automatically goes into a reduced phase fault-tolerant control. In Fig. 21 the electromagnetic torque is presented after the fault occurs at time 0.03 s, without mod-

ifying the DTC algorithm.

The next measurements of the fault-tolerant control were made with a modified DTC algorithm and without including the pre-firing angle (Fig. 22). Finally, the pre-firing angle was also included (Fig. 23). It can be noticed that the current and torque ripple at the experimental measurements are slightly larger than in simulations. The reason is that simulations do not include dead-time between switching transistors, transistor voltage drops, parasite influences, algorithm execution delay, etc. Nevertheless, the current ripple difference does not have an influence on the proposed SOPF detection, identification, and fault-tolerant control methods.
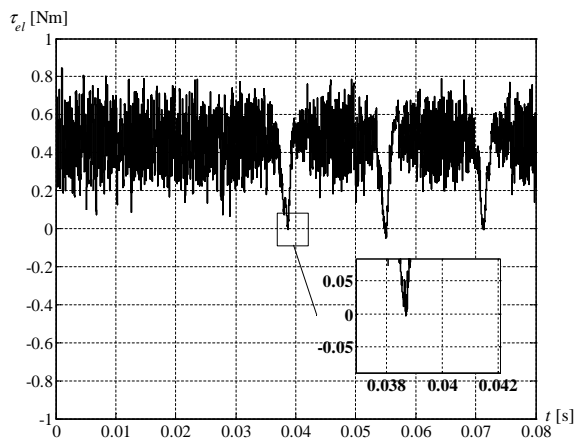
τ_{el} [Nm]

Fig. 23. Measurement results of electromagnetic torque (SOPF occurs at 0.03 s) with a modified DTC algorithm and with the pre-firing angle included

to current measurement uncertainty. Also, predictive approach used for detection has proven to be robust [9,11]. Nevertheless, this will be addressed more carefully in future work.

Additionally, a fault-tolerant control strategy with reduced phases is proposed. The solution is very economical since the power converter topology does not change after fault detection; the change is required only in the control algorithm. Since in the case of a SOPF only two voltage vectors are available, the drive operates with reduced power and typical torque oscillation of a single-phase operation with twice the stator frequency, going down to zero. For better performance of the complete drive the pre-firing angle was also introduced in order to avoid the temporary production of negative torque. Another important advantage of the implementation of the pre-firing angle is the reduction in the mechanical stress on various machine parts, being evident in the reduction of noise produced by the machine operating in post-fault mode.

Indubitably, the proposed fault-tolerant control is not appropriate for the systems where torque oscillation is not allowed in any case. Usually, due to the inertia of the system, mechanical speed does not change significantly during one electrical period (e.g. electric traction, HVAC, etc.), therefore this method can be used in order to provide low-cost "fault tolerance" and the consequent safe stop of the drive. Future research work will be focused on implementing the "fault-tolerance" concept to the FOC.

Another important advantage of including the pre-firing angle is the reduction of noise. The noise was measured with 2310 SL sound level meter. With a healthy inverter the noise level was about 60 dBA. If a SOPF occurs and the DTC algorithm is not modified, the sound level meter showed 70 dBA. When operating with a modified DTC algorithm and without pre-firing, the amplitude of noise was at the level of 68 dBA. After including the pre-firing angle the noise amplitude reduced to 64 dBA. In addition to the noise reduction, the introduction of the pre-firing angle generally reduces the stress on key mechanical parts of the electrical machine.

9 CONCLUSION

In this paper a low-cost, fault-tolerant model of a PMSM drive has been presented. It includes the predictive method for single open-phase fault detection and low-cost fault-tolerant control. The major advantage of the proposed detection method is that a SOPF can be detected and identified in a few sampling intervals (few hundreds of μs). Computer simulations and experimental measurements were made for two completely opposite conditions, when one of the phases is opened at the maximum and at the minimum value of the current in the corresponding phase winding. A comparison between simulations and experimental measurements reveal very good matching. For both evaluated amplitudes of the phase current, a SOPF can be detected in a few sampling intervals, but in the case of maximum phase current the detection is more straightforward. At this stage no problems with the robustness of the method have been encountered, since the fault index is usually so high that it exceeds possible deviation due

REFERENCES

[1] I. Edward, S. Wahsh and M. A. Badr, "Analysis of PMSM Drives for Electric vehicles," in Proceedings of the 37th SICE Annual Conference in International Session Papers (SICE '98), 1998.

[2] P. C. Krause, O. Wasynczuk and S. D. Sudhoff, Analysis of Electric Machinery and Drive Systems. 2nd edition, 632 pages, 2002.

[3] X. Jiaqun, T. Renyuan, O. Minggao, "Improved Direct Torque Control of Permanent Magnet Synchronous Motor in Electric Vehicle Drive," in IEEE Vehicle Power and Propulsion Conference (VPPC '08), 2008.

[4] M. Merzoug, F. Naceri, "Comparison of Field-Oriented Control and Direct Torque Control for Permanent Magnet Synchronous motor (PMSM)," Proceedings of world academy of science, engineering and technology, vol. 35, pp. 299-304, 2008.

[5] X. del Toro Garcia, B. Zigmund, A. Terlizzi, R. Pavlanin and L. Salvatore, "Comparison between FOC and DTC Strategies for Permanent Magnet Synchronous Motors," Advances in Electrical and Electronic Engineering, vol. 5, pp. 76-82, May 2006.

[6] R. Souad and H. Zeroug, "Comparison between Direct Torque Control and Vector Control of a Permanent Magnet

Synchronous Motor Drive," in 13th Power Electronics and Motion Control Conference (EPE-PEMC), Sept. 2008.

[7] L. Zhong, M. F. Rahman, W. Y. Hu and K. W. Lim, "Analysis of Direct Torque Control in Permanent Magnet Synchronous Motor Drives," IEEE Transactions on Power Electronics, vol. 12, no. 3, pp. 528-536, 1997.

[8] Sikorski, Andrzej, and Marek Korzeniewski. "Improved Algorithms of Direct Torque Control Method." A Automatika–Journal for Control, Measurement, Electronics, Computing and Communications, vol. 54, no. 2, pp. 188-198, 2013.

[9] V. Ambrozic, K. Drobnic and M. Nemec, "Predictive Torque Control of Interior Permanent Magnets Synchronous Motors in Stator Co-ordinates," in IEEE International Symposium on Industrial Electronics (ISIE), Jun 2011.

[10] M. Pacas and J. Weber, "Predictive Direct Torque Control for the PM-Synchronous Machine," in the 29th Annual Conference of the IEEE Industrial Electronics Society (IECON '03), 2003.

[11] K. Drobnic, M. Nemec, D. Nedeljkovic and V. Ambrozic, "Predictive Direct Control Applied to AC drives and Active Power Filter," IEEE Transactions on Industrial Electronics, vol. 56, no. 6, pp. 1884-1893, Jun 2009.

[12] F. W. Fuchs, "Some Diagnosis Methods for Voltage Source Inverters in Variable Speed Drives with Induction Machines - A Survey," in the 29th Annual Conference of the IEEE Industrial Electronics Society (IECON '03), Nov. 2003.

[13] Y. Jeong, S. Sul, S. Schulz and N. Patel, "Fault Detection and Fault Tolerant Control of Interior Permanent Magnet Motor Drive System for Electric Vehicle," in Conference Record of the 38th Industry Applications Conference (IAS 2003), Oct. 2003.

[14] D. Kastha and B. K. Bose, "Investigation of Fault Modes of Voltage-Fed Inverter System for Induction Motor Drive," in Conference Record of the IEEE Industry Applications Society Annual Meeting, Oct 1992.

[15] T. Sun, S. Lee and J. Hong, "Faults Analysis and Simulation for Interior Permanent Magnet Synchronous Motor using Simulink@Matlab," in International Conference on Electrical Machines and Systems (ICEMS 2007), Oct. 2007.

[16] B. A. Welchko, T. A. Lipo, T. M. Jahns and S. E. Schulz, "Fault Tolerant Three-Phase AC Motor Drive Topologies: A Comparison of Features, Cost, and Limitations," IEEE Transactions on Power Electronics, vol. 19, no. 4, pp. 1108-1116, Jul 2004.

[17] B. Lu and S. Sharma, "A Literature Review of IGBT Fault Diagnostic and Protection Methods for Power Inverters," in IEEE Industry Applications Society Annual Meeting (IAS '08), Oct. 2008.

[18] N. M. A. Freire, J. O. Estima and A. J. Marques Cardoso, "Open-circuit Fault Diagnosis in PMSG Drives for Wind Turbine Applications," IEEE Transactions on Industrial Electronics, vol. 60, no. 9, pp. 3957-3967, 2013.

[19] D. U. Campos-Delgado, J. A. Pecina-Sanchez, D. R. Espinoza-Trejo and E. R. Arce-Santana, "Diagnosis of Open-Switch Faults in Variable Speed Drives by Stator Current Analysis and Pattern Recognition," IET Electric Power Applications, vol. 7, no. 6, 2013.

[20] S. Jung, J. Park, H. Kim, K. Cho and M. Youn, "An MRAS-based Diagnosis of Open-Circuit Fault In PWM Voltage-Source Inverters for PM Synchronous Motor Drive Systems," Power Electronics, IEEE Transactions on, vol. 28, no. 5, pp. 2514-2526, 2013.

[21] J. O. Estima and A. J. Marques Cardoso, "A New Algorithm for Real-Time Multiple Open-Circuit Fault Diagnosis in Voltage-Fed PWM Motor Drives by the Reference Current Errors," IEEE Transactions on Industrial Electronics, vol. 60, no. 8, pp. 3496-3505, 2013.

[22] J. O. Estima and A. J. Marques Cardoso, "A New Approach for Real-Time Multiple Open-Circuit Fault Diagnosis in Voltage-Source Inverters," IEEE Transactions on Industry Applications, vol. 47, no. 6, pp. 2487-2494, 2011.

[23] A. Khlaief, M. Boussak and M. Gossa, "Open Phase Faults Detection in PMSM Drives based on Current Signature Analysis," in XIX International Conference on Electrical Machines (ICEM), Sept. 2010.

[24] D. Sun and Y. He, "A Modified Direct Torque Control for PMSM under Inverter Fault," in Proceedings of the Eighth International Conference on Electrical Machines and Systems (ICEMS 2005), Sept. 2005.

[25] D. Sun and J. Meng, "Research on Fault Tolerant Inverter-Based Permanent Magnet Synchronous Motor Direct Torque Control Drives," in 1'st IEEE Conference on Industrial Electronics and Applications, May 2006.

[26] Y. Ivonne, D. Sun and Y. He, "Study on Inverter Fault-Tolerant Operation of PMSM DTC," Journal of Zhejiang University-Science A, vol. 9, no. 2, pp. 156-164, 2008.

[27] H. Lin, H. Li, Y. Wang, M. Li, P. Wen and C. Zhang, "On Inverter Fault-Tolerant Operation Vector Control of a PMSM Drive," in IEEE International Conference on Intelligent Computing and Intelligent Systems (ICIS 2009), Nov. 2009.

[28] M. Naidu, S. Gopalakrishnan, T. W. Nehl, "Fault-tolerant Permanent Magnet Motor Drive Topologies for Automotive X-By-Wire Systems," IEEE Transactions on Industry Applications, vol. 46, no. 2, pp. 841-848, 2010.

[29] R. R. Errabelli and P. Mutschler, "Fault-tolerant Voltage Source Inverter for Permanent Magnet Drives," IEEE Transactions on Power Electronics, vol. 27, no. 2, pp. 500-508, 2012.

[30] K. D. Hoang, Z. -. Zhu and M. Foster, "Direct Torque Control of Permanent Magnet Brushless AC Drive with Single-Phase Open-Circuit Fault Accounting for Influence of Inverter Voltage Drop," IET Electric Power Applications, vol. 7, no. 5, pp. 369-380, 2013.

[31] A. M. S. Mendes and A. J. M. Cardoso, "Fault-tolerant Operating Strategies Applied to Three-Phase Induction-Motor Drives," IEEE Transactions on Industrial Electronics, vol. 53, no. 6, pp. 1807-1817, Dec. 2006.

[32] J. O. Estima and A. J. M. Cardoso, "Fast Fault Detection, Isolation and Reconfiguration in Fault-Tolerant Permanent Magnet Synchronous Motor Drives," in IEEE Energy Conversion Congress and Exposition (ECCE 2012), 2012.

[33] M. Villani, M. Tursini, G. Fabri and L. Castellini, "Multiphase Fault Tolerant Drives for Aircraft Applications," in Electrical Systems for Aircraft, Railway and Ship Propulsion (ESARS 2010), 2010.

[34] J. Zhu, H. Zhang, R. Tang, "The Study and Modeling of Multi-Phase PMSM Variety Speed System with High Fault-Tolerant," in International Conference on Electrical Machines and Systems (ICEMS 2008), 2008.

[35] M. Jurkovic and D. Zarko, "Optimized Design of a Brushless DC Permanent Magnet Motor For Propulsion of an Ultra-Light Aircraft," Automatika–Journal for Control, Measurement, Electronics, Computing and Communications, vol. 53, no. 3, 2012.

[36] I. Takahashi and T. Noguchi, "A New Quick-Response and High-Efficiency Control Strategy of an Induction Motor," IEEE Transactions on Industry Applications, vol. IA-22, no. 5, pp. 820-827, 1986.

[37] A. Kontarcek, P. Bajec, M. Nemec and V. Ambrozic, "Predictive Current Method for Single Open-phase Fault Detection in Permanent Magnet Synchronous Machine," in 13th International Symposium "Topical Problems in the Field of Electrical and Power Engineering", Jan. 2013.

[38] M. Nemec, K. Drobnic, D. Nedeljkovic and V. Ambrozic, "Direct Current Control of a Synchronous Machine in Field Coordinates," IEEE Transactions on Industrial Electronics, vol. 56, no. 10, pp. 4052-4061, Oct. 2009.

[39] I. Bahun, N. Cobanov and Z. Jakopovic, "Real-time Measurement of IGBT's Operating Temperature," Automatika–Journal for Control, Measurement, Electronics, Computing and Communications, vol. 52, no. 4, pp. 295-305, 2012.

[40] A. Kontarcek, P. Bajec, M. Nemec and V. Ambrozic, "Operation of PMSM after Single Open-Phase Fault," in 8th International Conference-Workshop Compatibility and Power Electronics (CPE2013), Ljubljana, Slovenia, 2013.

Andraž Kontarček received the B.Sc. degree in electrical engineering from the Faculty of Electrical Engineering, University of Ljubljana, Ljubljana, Slovenia, in 2010. He is currently working toward the Ph.D. degree in the Faculty of Electrical Engineering. His main research interests include motor control, fault diagnostics in electric drives, and power electronics.

Mitja Nemec received the B.Sc. and Ph.D. degrees from the Faculty of Electrical Engineering, University of Ljubljana, Ljubljana, Slovenia, in 2003 and 2008, respectively. He is currently an Assistant Professor with the Faculty of Electrical Engineering, University of Ljubljana, where he is working in the area of power electronics and motion control. His main research interests include control of electrical drives, active power filters, and application of power electronics in automotive industry.

Primož Bajec was born in Ljubljana, Slovenia in 1974. He received the B.Sc., M.Sc. and Ph. D. degrees from the University of Ljubljana, Faculty of Electrical Engineering, in 1999 2002 and 2005, respectively. In 1999 he joined the Faculty of Electrical Engineering as a junior researcher. His main research interests included computer simulation in power electronics, solid-state power converters and control of electrical drives. He has participated in several R&D projects, especially in the area of electrified powertrain systems for automotive applications and electrical machine supervision. Since 2005 he is at Hidria Corporation, initially managing the R&D activities on various e-machine drive projects for automotive applications. Recently he is focused on industrialization projects and low-volume production of laminated cores for high-performance automotive electrical machines, implementing state-of-the-art manufacturing technologies.

Vanja Ambrožič received the B.S., M.S., and Ph.D. degrees from the Faculty of Electrical Engineering, University of Ljubljana, Slovenia, in 1986, 1990, and 1993, respectively. In 1986, he joined the Laboratory of Control Engineering at the same faculty, first as a Junior Researcher, then as an Assistant and Assistant Professor. He is currently Full Professor and Head of the Department of Mechatronics. His main research interests include control of electrical drives and power electronics.

AUTHORS' ADDRESSES

Andraž Kontarček, B.Sc.
Primož Bajec, Ph.D.
Hidria d.d.
Spodnja Kanomlja 23, SI-5281, Spodnja Idrija, Slovenia
email: andraz.kontarcek@hidria.com,
primoz.bajec@hidria.com
Asst. Prof. Mitja Nemec, Ph.D.
Prof. Vanja Ambrožič, Ph.D.
Department of Mechatronics,
Faculty of Electrical Engineering,
University of Ljubljana,
Tržaška c. 25, SI-1000, Ljubljana, Slovenia
email: mitja.nemec@fe.uni-lj.si, vanjaa@fe.uni-lj.si